American Mineralogist, Volume 88, pages 1471–1485, 2003

Experimental investigation of crystallization kinetics in a haplogranite system

SUSAN COUCH*

ABSTRACT

A haplogranite composition (73 wt% SiO_2) has been studied experimentally to investigate the kinetics of crystallization. A series of equilibrium experiments over a range of pressures (5–200 MPa) and temperatures (825–1185 °C) determined the stable phases at water-saturated conditions. The haplogranite system crystallizes plagioclase over a broad range of pressures and temperatures, with crystalline silica and then alkali feldspar becoming stable at progressively lower temperatures and pressures. Plagioclase An contents decrease and bulk crystal fractions increase as experimental conditions tend to lower pressures and temperatures. A second series of experiments investigated the kinetics of crystallization induced by depressurization and associated water exsolution. A nucleation delay of at least 4 hours is estimated for all final pressures (P_f) studied. The amount of crystallization increases as P_f decreases and experimental duration and undercooling increase. Nucleation and growth rates are observed to increase with undercooling, although at very high undercoolings, growth rates start to decrease. Comparison with other experimental studies shows the importance of composition and water content to nucleation and growth rates. Increasing water content lowers melt viscosity, aiding crystallization.

INTRODUCTION

The recent eruption of volcanoes such as Soufrière Hills Volcano (Montserrat), Mount Pinatubo (Philippines), and Mount St. Helens (U.S.A.) have all been characterized by dome-building activity. Dome-forming eruptions are often observed to have complicated, non-linear behavior, which is related to volatile loss, crystallization, and rheological stiffening during ascent (Eichelberger et al. 1986; Melnik and Sparks 1999; Sparks et al. 2000; Blundy and Cashman 2001). Water exsolution during ascent can alter the conditions of the phase boundaries for minerals such as plagioclase feldspar in water-saturated magmas. Magma that was at or above the plagioclase liquidus at elevated pressures can become significantly undercooled during decompression, causing extensive groundmass crystallization. The overall temperature of the magma is balanced by cooling due to exsolution of water from the melt (Sahagian and Proussevitch 1996; Zhang 1999; Mastin and Ghiorso 2001), with latent heat release during crystallization (Couch et al. 2003a). This crystallization, combined with the decreased water content of the melt phase, can cause the magma viscosity to increase by several orders of magnitude (Lejeune and Richet 1995; Sparks et al. 2000), which will have implications for eruptive style.

Crystallization during ascent is by definition confined to the period of time spent in the volcanic conduit or within the lava dome. The short duration of this phase combined with the extent of disequilibrium (i.e., high undercooling) imposed by water exsolution, results in the crystallization of numerous small crystals (Couch et al. 2003b). If ascent of magma is very rapid, magma can cross the glass transition temperature before any crystals can form (Cashman and Blundy 2000). Therefore, it is expected that changes in groundmass textures are likely to reflect variations in degassing style and magma ascent rate.

A haplogranite composition (73 wt% SiO_2) was selected for study, as many andesite and dacite magmas have a rhyolitic melt composition just prior to eruption [i.e., Mount St Helens (Rutherford et al. 1985; Soufrière Hills, Montserrat (Couch et al. 2003a); Fish Canyon (Bachmann et al. 2002)]. The haplogranite composition used was similar to the average granite composition of Nockholds (1954) that was experimentally investigated by Whitney (1975) and Swanson (1977). Swanson considered crystallization kinetics as a function of isobaric cooling. Charges of starting material were annealed at a high temperature before being rapidly cooled to the temperature of interest and left for an appropriate period of time. Hence, one aim of this study was to compare the kinetics of crystallization induced by decompression with the cooling experiments of Swanson. An advantage of the haplogranite is that it is intrinsically a simpler system than a natural composition, although the addition of minor components (e.g., MgO and FeO) may affect the crystallization kinetics (Naney and Swanson 1980).

The concept of decompression-induced crystallization is not new (Tuttle and Bowen 1958; Whitney 1975), however, it has only been in recent years that such crystallization has been reproduced experimentally. Such studies include dacites from Mount St Helens (Geschwind and Rutherford 1995) and Mount Pinatubo (Hammer and Rutherford 2002) and andesites of the Soufrière Hills, Montserrat (Couch et al. 2003b). This study seeks to provide further experimental data by using a rhyolitic composition and considering the influence of composition on the crystallization kinetics.

Equilibrium experiments were run to determine the phase

* E-mail: s.couch@mail.com
Work on this paper was carried out at the Department of Earth Sciences, University of Bristol, Bristol, BS8 1RJ, U.K. and the School of Environmental Science, University of East Anglia, Norwich, NR4 7TJ, U.K.

0003-004X/03/0010–1471$05.00

relations and position of the phase liquidi. Decompression experiments were then carried out to consider the kinetics of crystallization imposed by depressurization. These experiments investigated how crystallization kinetics are affected by different values of undercooling, and also to replicate eruptive processes. A single decompression represents a sudden change in pressure, which may occur after a major dome collapse or an explosion, and incremental decompression may simulate pulsating behavior that can occur during ascent in the volcanic conduit (i.e., Soufière Hills Volcano, Montserrat, Voight et al. 1999; Wylie et al. 1999).

METHODS

Equilibrium experiments

The starting composition, a haplogranite, was prepared from reagent-grade carbonates and oxides that were dried before weighing, ground in an agate mortar, slowly decarbonated, and heated to 1650 K in a platinum crucible in an electric furnace, quenched, and ground. This procedure was repeated four times. The composition differs slightly from that used by Swanson (1977) (Table 1). The differences were probably introduced during the preparation of the starting composition glass. 0.05 g of finely ground starting material was placed inside 2.5 mm diameter $Ag_{75}Pd_{25}$ capsules, with sufficient H_2O to ensure water saturation at the pressure-temperature (*P-T*) conditions. After welding, the capsules were heated briefly to check they were sealed. All experiments were carried out in rapid-quench cold-seal pressure vessels (Carroll and Blank 1997), with an H_2O pressurizing fluid at pressures of 5 to 200 MPa. P. Rouse (personal communication) determined the oxygen fugacity of the cold seal set-up to be NNO +1.3 based on co-existing NiO-NiPd alloys (Taylor et al. 1992).

Temperature was measured by K-type (chromel-alumel) thermocouples, precise to ±5 °C, with accuracy checked by B-type ($Pt_{94}Rh_6$-$Pt_{70}Rh_{30}$) thermocouples, calibrated at the melting point of gold (Gardner et al. 2000). Pressure was measured by either Nova Swiss static pressure gauges, precise to ±2.5 MPa, or by a pressure transducer, precise to <1 MPa. The experiments were left for 1 to 14 days to equilibrate, and were then quenched rapidly. To test the approach to equilibrium, several reversal experiments were performed. A sample was taken to higher pressure for several hours, before being adjusted to the desired *P-T* conditions and left for an appropriate time period. The nucleation of plagioclase was sluggish close to the liquidus, and therefore seeds of finely ground andesine (An_{30}) were added to high *P-T* experiments (Table 1).

TABLE 1. Haplogranite used by Swanson (1977), starting composition for this experimental study and andesine seed composition

Wt% oxides	Haplogranite Swanson (1977)	Starting composition	1σ
SiO_2	73.98	73.03	0.7
Al_2O_3	15.07	15.87	0.6
CaO	1.50	1.66	0.2
Na_2O	3.75	3.79	0.2
K_2O	5.70	5.65	0.1
Wt% oxides	Andesine seed composition	1σ	
SiO_2	60.22	0.51	
TiO_2	0.03	0.03	
Al_2O_3	25.11	0.28	
FeO	0.05	0.04	
MgO	0.04	0.03	
CaO	6.13	0.20	
Na_2O	7.73	0.37	
K_2O	0.31	0.04	
Total	99.62	0.71	
Total	4.99	0.02	
Ab	68.26	1.52	
An	29.94	1.44	
Or	1.80	0.20	

Note: Starting composition renormalized to 100% anhyrdous.

Decompression experiments

A second series of experiments investigated the kinetics of plagioclase crystallization in response to depressurization. These experiments were run in the same apparatus as the equilibrium experiments. All runs experienced a pre-decompression step at 875 °C and PH_2O of 160 MPa for 16 hours. These conditions are approximately at the plagioclase liquidus at 160 MPa if the melt is water-saturated. The crystallization of plagioclase within the haplogranite was found to be sluggish and, therefore, all the decompression experiments contained ~5 µg of andesine seeds to aid nucleation. These seeds were clearly distinguished from plagioclase crystals associated with new growth, being both morphologically and compositionally distinct. It is possible that the addition of these plagioclase seeds could change the bulk composition and affect the experimental results. However the seeds comprise ~1% of the total starting material and are therefore unlikely to significantly alter the bulk composition.

After annealing, the experimental charge was decompressed. Depressurization was controlled by a manually operated piston-screw pump, which enabled near-instantaneous decompressions. Decompression induces an undercooling (ΔT) calculated from the equilibrium plagioclase liquidus. As the final pressure (P_f) decreases, ΔT increases.

Two types of experiments were carried out: single-decompression experiments (SDE) and multi-step decompression experiments (MDE). SDE experiments involved depressurization from 160 to 125, 100, 75, 50, or 30 MPa, which impose a ΔT of 35, 60, 89, 123, or 167 °C (±10 °C), respectively. The depressurization step was complete in less than 1 minute. After decompression, the pressure line was closed and the experiment left to run for periods ranging from 1 to 504 hours (3 weeks) and then quenched. For the MDE experiments, the total pressure change from the anneal pressure of 160 MPa to the final pressure (125, 100, 75, or 50 MPa) was divided into 8 equal decompression steps. The sample was left for a fixed period (1 h, 12 h, 24 h) between each step. By varying the duration between steps, a range of ascent rates for the experiments is estimated to vary from ~2 – 0.002 m/s. These rates are similar to with those calculated for dome-forming eruptions such as Mount St. Helens and Soufrière Hills, Montserrat (Geschwind and Rutherford 1995; Rutherford et al. 1998).

Analytical techniques

Polished and carbon-coated thin sections of experiments and natural samples were analyzed at University of Bristol on a Cameca Camebax microprobe using SamX software with PAP correction procedures for plagioclase, and a JEOL JXA8600 microprobe with ZAF correction procedures for glass, at 15 kV accelerating voltage. The JEOL instrument was used for glass analyses as it has 4 spectrometers enabling analysis to be completed quickly, before significant alkali loss occurred. Crystals were analyzed with a 10 nA beam current and a 1 µm stationary beam, and glass at 2 nA with a 10 µm rastered beam, again to minimize alkali mobility as discussed in Couch et al. (2003a). Calibration used known standards (albite for Na and Si; Al_2O_3 for Al; sanidine for K and andradite for Ca) and then was checked by analysis of the secondary standards Kakanui Kaersutite (KK1) and Comenditic obsidian (Kn18). Typically, 5–10 plagioclase analyses were carried out for each experiment, and ~5 analyses for all other phases. For the equilibrium experiments, the proportions of phases were determined using the mass-balance PETMIX program (Wright and Doherty 1970). Analysis of cores and rims of plagioclase microlites was carried out for the decompression experiments, and the length and width of the crystal measured.

Image analysis

I measured plagioclase proportions and crystal dimensions on five backscattered electron images at different scales for each decompression sample using a Cambridge Stereoscan MK250 Scanning Electron Microscope. Plagioclase fraction (ϕ) and number density (number/mm^2, N_a) were determined, using similar methods to Hammer et al. (1999). Typically, about 50 crystals per field of view were measured, although the count was lower in some low crystallinity samples. Crystals that were cut by the image edge were included in the count of nucleation sites. Crystals that were skeletal or spherulitic were considered as a single nucleation site. Determination of nucleation sites in high ΔT experiments was difficult due to the dendritic morphology of the crystals.

Characteristic crystal size, s (mm), and the volumetric number density, N_v (1/mm^3) were calculated from:

$$s = \left(\frac{\phi}{N_a}\right)^{1/2} \quad (1)$$

$$N_v = \frac{N_a}{s} \quad (2)$$

Crystal sizes were adjusted for stereological effects, assuming an approximately spherical shape (Kellerhals et al. 1975; Weibel 1980). The N_v calculation uses a standard method for correcting the area- to volumetric- density (Cheng and Lemlich 1983). The incremental nucleation rate, I_i (1/mm^3 s), can be estimated from:

$$I_i = \frac{N_{vb} - N_{va}}{t_b - t_a} \quad (3)$$

Here N_{vb} and N_{va} are the nucleation densities at times t_a and t_b for two experiments with the same ΔT and different durations. As duration increases, the overall number of nucleation sites should remain constant, or should increase. Due to experimental scatter, lines of best fit were plotted and used to calculate s and N_v as functions of time. The incremental nucleation rate was calculated only for SDE. For the MDE, a time-averaged, and therefore minimum rate, I_m, was calculated, where:

$$I_m = \frac{N_v}{t} \quad (4)$$

Here t is the total experiment duration.

Incremental growth rate, G_i, is approximated as the average of the half-length (L) of the ten longest plagioclase crystals, as employed by Fenn (1977) and Hammer and Rutherford (2002);

$$G_i = \frac{0.5L_b - 0.5L_a}{t_b - t_a} \quad (5)$$

where t_a and t_b are the duration of each experiment. Crystals that touched the image edge were not included and, due to experimental scatter, lines of best fit were plotted and used to calculate the half-length. For the MDE, a time-averaged growth rate, G_m, was calculated:

$$G_m = \frac{0.5L}{t} \quad (6)$$

Maximum overgrowth rim width was determined by measuring all overgrowths observed in an image and selecting the highest value.

Hammer et al. (1999) compared the techniques used in CSD analysis and found similar overall results, with the advantage of allowing analysis of more samples than by CSD analysis. Furthermore, stereological corrections are needed for CSD analysis, which is difficult for the hopper, swallowtail, and skeletal morphologies commonly encountered in the experiments (Hammer and Rutherford 2002).

Experimental results for equilibrium experiments

A summary of the key experimental results is shown in Table 2. For selected experimental conditions, reversal experiments were run to check that equilibrium was approached. There is relatively good agreement between the two types of experiments, especially in plagioclase anorthite content.

SEM images of the experimental charges show that there is a systematic variation in the morphology of the plagioclase crystals with tabular crystals at the highest pressures and temperatures and a trend of hopper, skeletal, spherulitic and dendritic at increasingly low pressures and temperatures (Fig. 1). The number density of plagioclase crystals increases as pressure and temperature decrease. The nucleation of feldspar around small crystalline silica grains (Fig. 1a) is very similar to textures seen in Mount St Helens dacites (see Fig. 6h from Blundy and Cashman 2001).

Stable phases and compositional trends

The phase relations have been determined (Fig. 2) with plagioclase stable to high pressures and temperatures. The phase diagram shows considerable similarity to those constructed by Whitney (1975) using a similar starting composition. Crystalline silica is stable at lower temperatures, and alkali feldspar is found at the lowest pressures and temperatures. At very low *P-T* conditions, plagioclase feldspar was impossible to analyze as the crystals were very thin (~2 μm in width) and difficult to distinguish from the glass. Radiating spherulitic crystals can be observed (Fig. 1a), which are interpreted as plagioclase, and lighter grey, more tabular crystals as alkali feldspar. For the equilibrium experiments that were seeded, the presence or absence of overgrowth rims on the seeds defined whether the plagioclase liquidus had been reached.

The plagioclase anorthite content shows systematic variation with pressure and temperature (Fig. 2). The highest anorthite contents are observed at high *P-T* conditions, with a trend of decreasing An content with decreasing *P-T*. The glass compositions (Table 3) can provide information about which phases are crystallizing. Glass compositions have been renormalized by projecting from anorthite and plotted onto the quartz-albite-orthoclase ternary (Fig. 3) of Blundy and Cashman (2001), which is based on Tuttle and Bowen (1958). Three main compositional groups are observed. For those experiments that did not crystallize a silica phase (high *P-T*), compositions track away from the starting composition toward the Qz'-Or' cotectic. At lower pressures and temperatures, silica is crystallized and the melt composition is displaced away from the first group, along the quartz-orthoclase cotectic. When alkali feldspar becomes a stable phase, together with crystalline silica and plagioclase, the melt compositions are displaced toward the quartz apex. The evolved nature of this last group of melts confirms that plagioclase feldspar must have crystallized extensively, although crystals of plagioclase could not be analyzed. The very low pressure experiments can be used to define the 25 MPa ternary minimum, which follows the trend of higher pressure minima curves from Blundy and Cashman (2001).

Experimental results for decompression experiments

The initial high-pressure conditions of 875 °C and 160 MPa are ~6 °C below the experimentally determined plagioclase liquidus (Fig. 2). Textural and compositional data suggest that no crystallization takes place during the initial high-pressure stage, probably due to the sluggish nature of the system. Therefore, even though the melt is slightly undercooled before decompression, the lack of crystallization means that ΔT can be calculated using the plagioclase liquidus derived from the equilibrium experiments. Rarely, crystals of plagioclase formed during annealing are observed, and they are distinguished by their high anorthite content relative to seed crystals (~An_{30}) and more tabular morphology relative to decompression-induced crystals. A summary of the major experimental results is shown in Table 4.

An important consideration for estimating crystallization kinetics due to depressurization is it to determine the time-scale of water exsolution relative to the experimental duration. Water saturation was achieved, as vesicles were observed in all experiments. As discussed in Couch et al. (2003b), the distance between bubbles can be used to estimate the time for equilib-

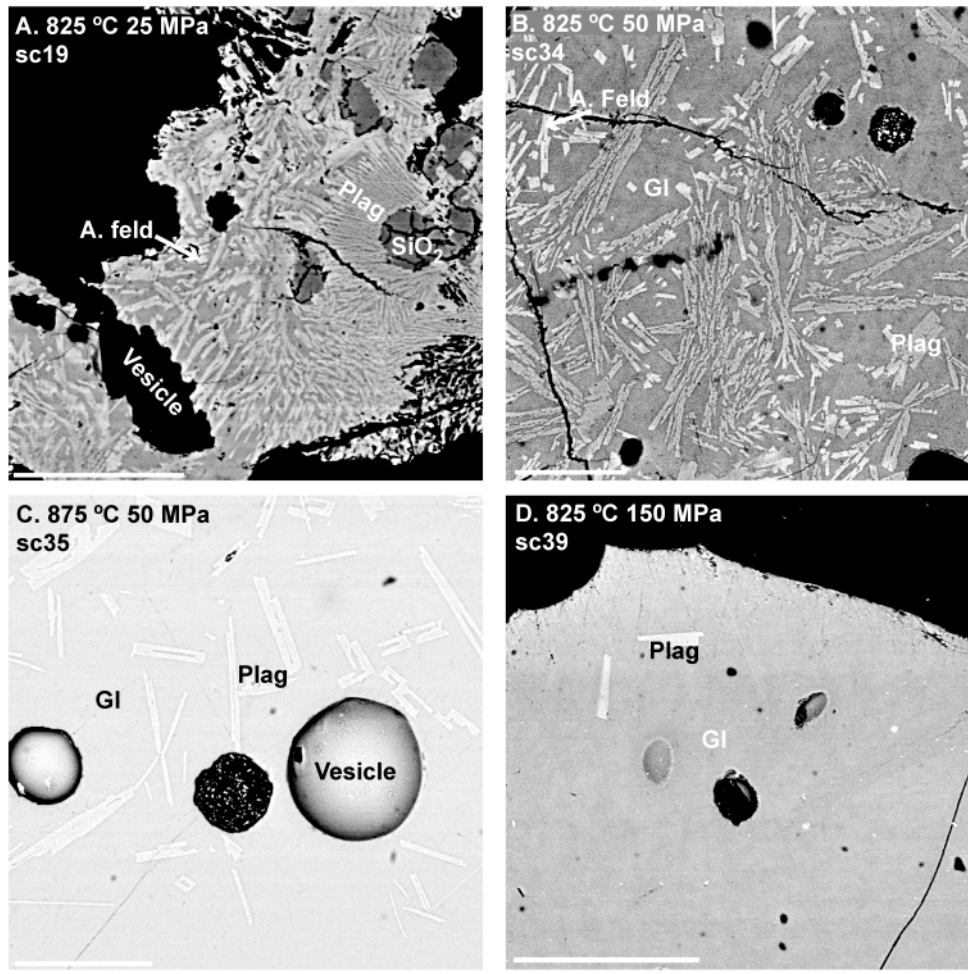

FIGURE 1. Back-scattered electron images of equilibrium experiments with experimental conditions as labeled. Pl = plagioclase; A.feld = alkali feldspar; Gl = glass**.** There is a systematic variation in plagioclase morphology; as pressure and temperature decrease, crystals change from tabular, to hopper, skeletal, spherulitic, and finally dendritic. Scale bar of 50 μm is shown.

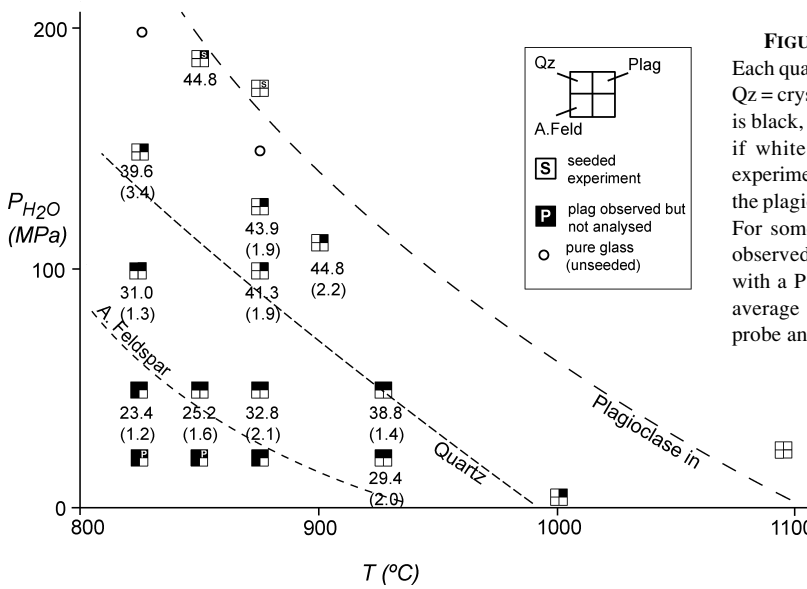

FIGURE 2. Phase diagram for haplogranite composition. Each quarter represents a different phase. Plag = plagioclase; Qz = crystalline silica; A.Feld = alkali feldspar. If the quarter is black, the phase is present at the experimental conditions; if white, the phase was not observed. Some unseeded experiments did not crystallize, even though they were below the plagioclase liquidus, and are labeled with an open circle. For some low *P-T* experiments, plagioclase feldspar was observed in the images but could not be analyzed, as labeled with a P in the plagioclase quarter. Beneath the box is the average plagioclase anorthite content (and 1σ) of several probe analyses.

TABLE 2A. Experimental summary for equilibrium experiments using haplogranite

Sample number	Temperature (°C)	Pressure (MPa)	ΔT (°C)†	Quartz present?	Crystal fraction (wt%)‡	Glass fraction (wt%)‡	Plagioclase fraction (wt%)‡	Plagioclase anorthite content§
sc41	1000	5	66	N	n.d.	n.d.	n.d.	
sc18	850	25	189	Y	82.16	17.84	n.d.	–
sc17	875	25	165	Y	n.d.	n.d.	n.d.	–
sc13	925	25	110	Y	17.18	82.82	17.17	29.4 (2.0)
sc82	1185	25	–	N	0	100	0	–
sc34	825	50	173	Y	46.13	53.87	22.92	23.5 (1.2)
sc36	850	50	149	Y	23.82	76.18	23.37	25.3 (1.6)
sc35	875	50	123	Y	19.12	80.88	19.12	32.8 (2.2)
sc33	925	50	73	Y	15.92	84.08	15.92	38.8 (1.4)
sc46	825	100	113	Y	18.73	81.27	18.73	31.1 (1.3)
sc45	875	100	60	N	9.48	90.52	9.48	41.3 (2.0)
sc55	900	110	24	N	7.73	92.27	7.73	44.8 (2.2)
sc37	875	125	33	N	7.41	92.59	7.41	43.9 (1.9)
sc39	825	150	61	N	8.63	91.37	8.63	39.6 (3.4)
sc56	875	150	11	N	0	100	0	–
sc89*	875	175	–	N	0	100	0	–
sc90*	850	185	5	N	7.65	92.35	7.65	44.8 (–)
sc44	825	200	22	N	7.32	92.68	7.32	39.3 (1.2)

Notes: n.d. = Not determined; – = Not applicable; phase not observed.
* Seeded experiment.
† Undercooling determined from experimentally derived plagioclase liquidus.
‡ Determined by mass balance (PETMIX, Wright and Doherty 1970) using average compositional data for phases.
§ Average (and 1σ) of several analyses.

TABLE 2B. Experimental summary for reversal experiments using haplogranite

Sample number	Temperature (°C)	Pressure (MPa)	ΔT (°C)†	Quartz present?	Crystal fraction (wt%)‡	Glass fraction (wt%)‡	Plagioclase fraction (wt%)‡	Plagioclase anorthite content§
sc67	875	50	123	Y	15.55	84.45	15.55	33.0 (2.8)
sc241	875	100	60	N	11.46	88.54	11.46	44.1 (1.0)

* Seeded experiment.
† Undercooling determined from experimentally derived plagioclase liquidus.
‡ Determined by mass balance (PETMIX, Wright and Doherty 1970) using average compositional data for phases.
§ Average (and 1σ) of several analyses.

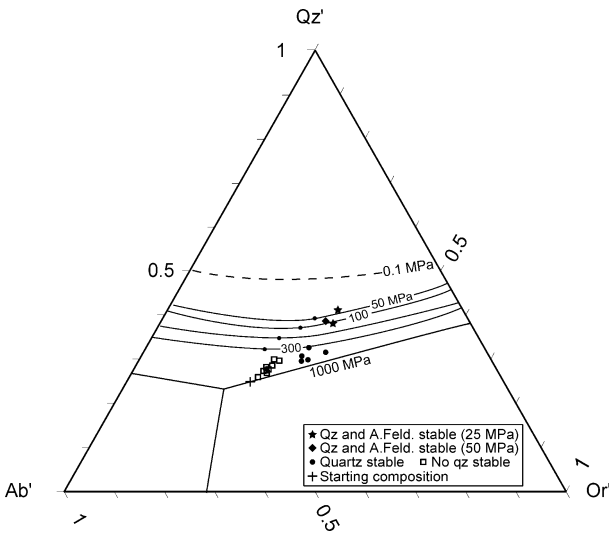

FIGURE 3. Ternary diagram of experimental glass compositions for equilibrium experiments. Qz'-feldspar (Ab'-Or') cotectic lines are shown, based on Blundy and Cashman (2001).

rium by a diffusional length-scale (Navon and Lyakhovsky 1998),

$$\delta \leftrightarrow 4Dt$$

where D is the water diffusion coefficient and t is time. With an observed distance of up to 80 μm between vesicles and a water diffusion coefficient of 10^{-7}–10^{-8} cm^2/s (Shaw 1974; Delaney and Karsten 1981), diffusion of H_2O should reach equilibrium from ~160 s to 25 minutes. The slowest rate to reach equilibrium may only be relevant to the very low pressure experiment (P_f = 30 MPa). Overall, the haplogranite system can be considered to exsolve H_2O on a time-scale much shorter than the experimental durations.

Experimental water contents can be estimated using the by-difference method (Devine et al. 1995) with compositional glass data. These estimations are compared with predicted water contents for a rhyolite at 850 °C (Silver et al. 1990). The SDE consistently have slightly higher H_2O contents than expected, and the MDE show unsystematic variation in H_2O content (Fig. 4). The error bars are based on the deviation around the mean value for each analysis, and are likely to be greater when errors for the by-difference method are added. There is also likely to be a further error from the small amount of Na loss (<5%) that occurs during glass analysis. Based on these additional errors in the water content estimation, the water content is close to the predicted value at a given pressure. These data confirm that the H_2O exsolution occurred on time-scales less than the shortest experiment.

Back-scattered electron SEM images of selected SDE and MDE experiments are shown in Figure 5. Seed crystals can clearly be identified (Fig. 5a, 5e, and 5f), as they are generally larger and more irregular in morphology, and in some experiments, they show overgrowth rims. As P_f decreases and ΔT

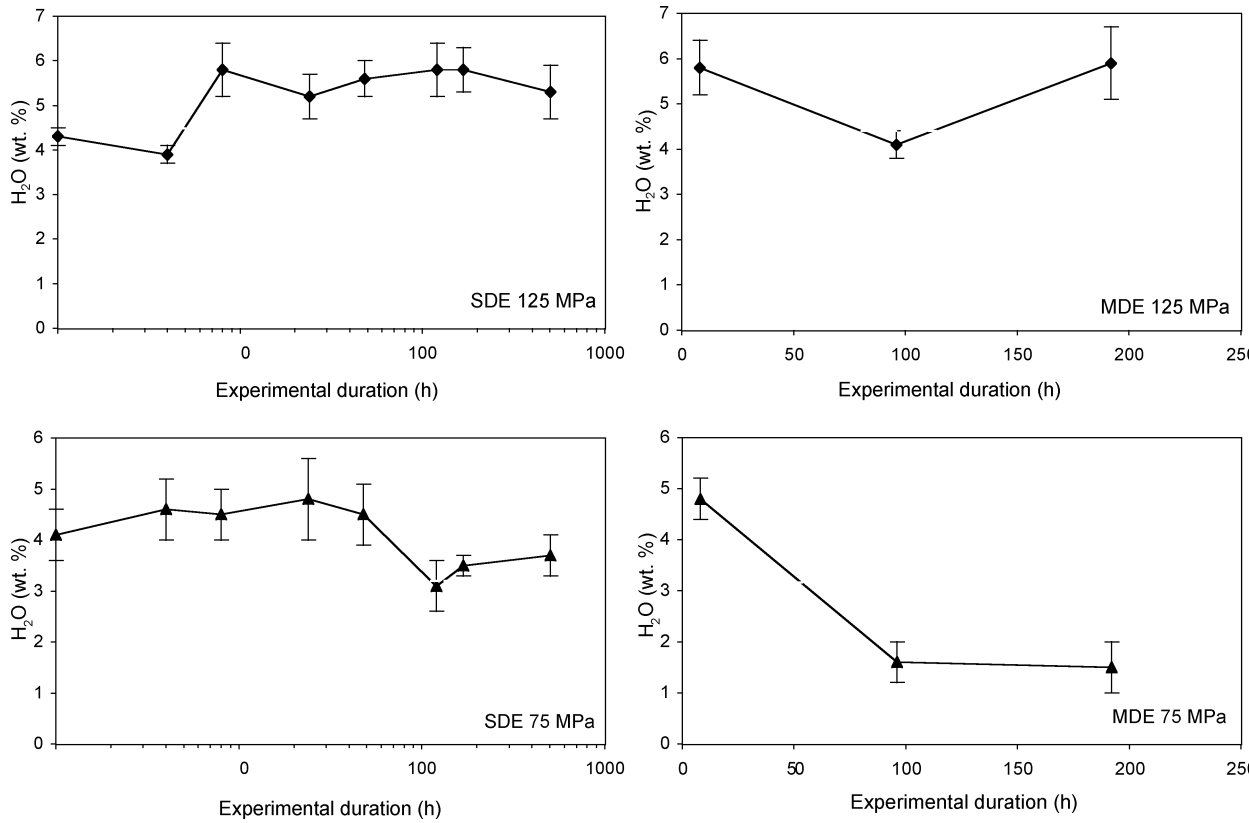

FIGURE 4. Graphs of H_2O content of melt with experimental duration and P_f for the decompression experiments. The dashed line is the equilibrium water content, estimated using Silver et al. (1990). (±1σ of mean water content shown) Experimental water content estimated using by-difference method from the average of several probe analyses (Table 5).

TABLE 3. Glass compositions for equilibrium experiments, normalized to 100% anhydrous. Average (and 1σ) of several analyses.

Sample	Temperature (°C)	Pressure (MPa)	No. of analyses	wt% SiO_2	wt% Al_2O_3	wt% CaO	wt% Na_2O	wt% K_2O	Unnormalized total (wt%)
Starting composition		-	13	73.03 (0.74)	15.87 (0.61)	1.66 (0.19)	3.79 (0.23)	5.65 (0.13)	99.25 (0.94)
sc18	850	25	9	79.60 (0.61)	11.55 (0.26)	0.43 (0.05)	2.50 (0.21)	5.84 (0.11)	96.77 (0.86)
sc17	875	25	9	78.46 (0.57)	12.22 (0.46)	0.46 (0.10)	2.69 (0.20)	6.05 (0.07)	97.60 (0.45)
sc13	925	25	11	75.32 (0.61)	14.20 (0.62)	0.76 (0.09)	3.40 (0.27)	6.21 (0.09)	97.25 (0.83)
sc82	1185	25	7	74.37 (0.47)	14.77 (0.50)	1.42 (0.17)	3.57 (0.18)	5.80 (0.12)	96.87 (0.56)
sc34	825	50	8	78.65 (0.87)	12.17 (0.19)	0.54 (0.05)	2.75 (0.13)	5.80 (0.09)	96.50 (0.89)
sc36	850	50	2	75.66 (0.27)	14.06 (0.17)	0.66 (0.10)	2.84 (0.04)	6.66 (0.02)	96.21 (0.03)
sc35	875	50	11	76.05 (0.74)	13.63 (0.19)	0.80 (0.07)	3.35 (0.27)	6.07 (0.04)	97.24 (0.67)
sc33	925	50	4	75.65 (0.17)	13.72 (0.28)	0.93 (0.06)	3.34 (0.08)	6.33 (0.02)	98.96 (0.28)
sc46	825	100	8	76.17 (0.74)	13.77 (0.20)	0.89 (0.04)	2.96 (0.36)	6.12 (0.08)	94.03 (0.78)
sc45	875	100	13	74.92 (0.67)	14.66 (0.36)	1.27 (0.08)	3.34 (0.08)	5.76 (0.10)	94.03 (0.66)
sc55	900	110	7	74.50 (0.79)	14.75 (0.34)	1.40 (0.08)	3.53 (0.19)	5.75 (0.08)	93.82 (1.03)
sc37	875	125	5	74.40 (0.58)	14.90 (0.55)	1.38 (0.08)	3.37 (0.19)	5.77 (0.13)	93.63 (0.70)
sc39	825	150	5	74.54 (0.29)	14.65 (0.29)	1.36 (0.07)	3.60 (0.10)	5.76 (0.08)	92.31 (0.37)
sc56	875	150	7	74.39 (0.38)	14.86 (0.33)	1.43 (0.09)	3.58 (0.22)	5.72 (0.07)	93.50 (0.68)
sc89*	875	175	7	73.91 (0.46)	15.05 (0.19)	1.54 (0.06)	3.78 (0.12)	5.73 (0.18)	93.40 (0.70)
sc90*	850	185	6	74.52 (0.80)	14.85 (0.38)	1.44 (0.09)	3.52 (0.20)	5.62 (0.12)	92.68 (0.47)
sc44	825	200	7	74.50 (0.24)	15.19 (0.12)	1.44 (0.04)	3.22 (0.16)	5.60 (0.10)	92.32 (0.47)

Note: Seeded experiments denoted by *.

increases, the morphology of the decompression-induced plagioclase crystals becomes increasingly skeletal. The number density of crystals also increases with ΔT.

Stable phases and compositional trends

In all the decompression experiment runs, plagioclase feldspar was the only phase that crystallized. Comparison of the anorthite content trends of the equilibrium experiments with the decompression experiments shows without exception that the decompression experiments crystallize plagioclase of higher anorthite content than equilibrium experiments at the same final pressure (Fig. 6). The SDE generally crystallize plagioclase with a higher anorthite content than the MDE.

Variations in glass composition are plotted on ternary dia-

TABLE 4. Summary of experimental results for decompression experiments using haplogranite composition

Sample no.	P_i (MPa)	ΔT (°C)	Duration at P_i (h)	IDR* (MPa/h^{-1})	Vol% plagioclase†	An content of new growth plag.‡	Crystal density§ (sites/mm^{-2})	Max. crystal length# (μm)	Max. growth rate** (mm/s^{-1})
					(a) SDE				
214	125	35	1	35.0	–	n.a.	n.a.	n.a.	n.a.
213	125	35	4	8.8	–	43.8 (3.3)	n.a.	n.a.	n.a.
177	125	35	8	4.4	0.2 (0.3)	48.2 (1.0)	14 (17)	31.27 (25.7)	4.49E-07
176	125	35	24	1.5	0.1 (0.1)	42.1 (0.9)	5 (5)	12.66 (3.8)	6.48E-08
157	125	35	48	0.7	0.2 (0.1)	43.2 (2.2)	23 (21)	18.37 (12.5)	2.73E-08
147	125	35	120	0.3	0.3 (0.4)	45.1 (1.3)	31 (29)	28.27 (20.3)	1.20E-08
148	125	35	168	0.2	–	41.6 (-)	n.a.	n.a.	6.62E-09
165	125	35	504	0.1	1.1 (0.5)	47.6 (0.4)	182 (102)	47.30 (12.1)	3.09E-09
215	100	60	1	60.0	0.4 (0.3)	n.a.	92 (56)	n.a.	n.a.
156	100	60	4	15.0	0.0 (0.0)	44.7 (3.1)	15 (29)	n.a.	n.a.
97	100	60	8	7.5	0.3 (0.2)	41.0 (–)	154 (146)	23.21 (5.7)	7.87E-07
98	100	60	24	2.5	4.4 (3.3)	37.3 (1.0)	887 (585)	50.85 (11.9)	1.32E-07
142	100	60	48	1.3	0.5 (0.4)	44.4 (2.0)	39 (41)	34.36 (10.5)	5.57E-08
137	100	60	120	0.5	1.7 (0.7)	43.8 (1.3)	96 (24)	64.25 (5.6)	2.46E-08
138	100	60	168	0.4	5.5 (2.1)	42.3 (1.9)	441 (251)	72.21 (11.8)	1.35E-08
164	100	60	504	0.1	2.5 (1.5)	45.8 (1.0)	117 (53)	75.49 (16.6)	6.31E-09
153	75	89	1	85.0	0.2 (0.5)	40.5 (–)	19 (43)	n.a.	n.a.
119	75	89	4	21.3	0.5 (0.4)	39.4 (3.7)	30 (22)	n.a.	n.a.
120	75	89	8	10.6	0.8 (0.6)	40.7 (–)	54 (80)	13.27 (4.0)	8.15E-07
121	75	89	24	3.5	2.8 (2.0)	37.0 (1.4)	491 (413)	48.17 (9.8)	1.61E-07
183	75	89	48	1.8	2.3 (2.3)	38.5 (2.8)	161 (122)	57.68 (7.1)	6.79E-08
122	75	89	120	0.7	5.4 (1.4)	37.2 (1.8)	288 (206)	70.09 (14.0)	2.99E-08
113	75	89	168	0.5	5.8 (1.7)	41.4 (2.0)	411 (170)	72.33 (12.3)	1.65E-08
163	75	89	504	0.2	9.0 (1.9)	42.2 (1.5)	377 (59)	95.64 (16.1)	7.69E-09
127	50	123	1	110.0	n.a.	n.a.	4 (9)	n.a.	n.a.
128	50	123	4	27.5	n.a.	42.8 (2.9)	5 (12)	n.a.	n.a.
103	50	123	8	13.8	2.1 (2.5)	n.d.	355 (375)	36.75 (17.5)	8.51E-07
104	50	123	24	4.6	6.2 (2.6)	32.9 (2.1)	1926 (765)	26.14 (6.2)	1.51E-07
129	50	123	48	2.3	5.2 (1.3)	34.9 (1.0)	517 (108)	61.35 (15.2)	6.35E-08
231	50	123	120	0.9	3.8 (1.1)	35.3 (1.1)	373 (131)	57.73 (9.1)	2.80E-08
228	50	123	168	0.7	3.7 (1.3)	31.4 (3.2)	240 (44)	76.55 (16.7)	1.54E-08
230	50	123	504	0.2	11.7 (0.8)	34.3 (1.2)	465 (103)	95.92 (23.7)	7.18E-09
232	30	167	8	16.3	0.6 (0.8)	n.d.	228 (200)	17.32 (16.1)	6.01E-07
					(b) MDE				
193	125	35	8	4.38	0.1 (0.1)	47.8 (2.1)	n.a.	n.a.	n.a.
220	125	35	96	0.36	0.4 (0.6)	46.6 (5.8)	n.a.	n.a.	n.a.
202	125	35	192	0.18	0.8 (0.7)	45.4 (–)	79 (57)	18.43 (11.8)	1.33E-08
200	100	60	8	7.50	0.2 (0.2)	49.1 (3.1)	8 (10)	6.56 (4.2)	1.14E-07
221	100	60	96	0.63	0.1 (0.2)	45.7 (2.9)	3 (4)	13.12 (6.5)	3.80E-08
206	100	60	192	0.31	2.3 (0.6)	42.7 (1.5)	150 (120)	19.73 (5.5)	1.43E-08
199	75	89	8	10.63	0.4 (0.3)	44.4 (3.2)	26 (16)	17.24 (10.4)	2.99E-07
239	75	89	96	0.89	2.0 (4.2)	45.7 (1.7)	82 (45)	28.35 (11.2)	8.20E-08
238	75	89	192	0.44	1.6 (0.7)	40.4 (1.5)	79 (44)	52.15 (15.3)	3.77E-08
227	50	123	8	13.75	0.6 (0.8)	37.3 (–)	77 (79)	7.72 (1.6)	2.75E-07
240	50	123	96	1.15	1.0 (0.7)	33.3 (3.8)	49 (49)	27.2 (12.3)	7.87E-08
207	50	123	192	0.57	5.3 (1.1)	41.7 (3.5)	386 (65)	63.92 (26.2)	4.62E-08
					(c) Repeat experiments				
137	Single-step	60	120	0.5	1.7 (0.7)	43.8 (1.3)	96 (24)	64.25 (5.6)	2.46E-08
244	Single-step	60	120	0.5	0.3 (0.2)	44.8 (2.0)	28 (17)	38.41 (19.3)	2.21E-08
227	Multi-step	123	8	13.75	0.6 (0.8)	37.3 (–)	77 (79)	7.72 (1.6)	1.34E-07
246	Multi-step	123	8	13.75	0.2 (0.3)	38.7 (1.4)	3 (7)	15.85 (–)	2.75E-07

* Integrated decompression rate; ΔP total/duration of experiment.
† Proportion of plagioclase; average (and 1σ) of area % plagioclase calculated from 5 images.
‡ Anorthite content of decompression induced plagioclase growth; average (and 1σ).
§ Nucleation density; average (and 1σ) calculated from 5 images.
# Maximum crystal length; average (and 1σ) calculated from the average of the 10 longest observed new crystals.
** Maximum growth rate; calculated using the half-length of the 10 longest crystals. Estimated as an incremental growth rate for SDE, time-averaged for MDE. Due to scatter in data, best fit lines were used to determine the trend of maximum length with time, and hence no errors are included.

grams (Fig. 7) and both SDE and MDE follow the same trend, moving away from the starting composition toward the Qz' apex. There is considerably less variation in melt composition than observed in the equilibrium experiments (Fig. 3), suggesting a more limited range of crystallization. No stable crystalline silica phase was observed in the experiments, and the glass trends on the ternary diagrams support this observation, as there is no displacement along the quartz-albite cotectic.

TEXTURAL RESULTS

Plagioclase fraction. Image analysis of experimental samples shows that the fraction of plagioclase increases with both ΔT and experimental duration (Fig. 8). There is considerable scatter in the data, relating to the heterogeneity of crystallization. In the case of the SDE run at ΔT = 35 °C, there is negligible crystallization regardless of length of experiment. For moderate undercoolings of 60–89 °C, crystallization com-

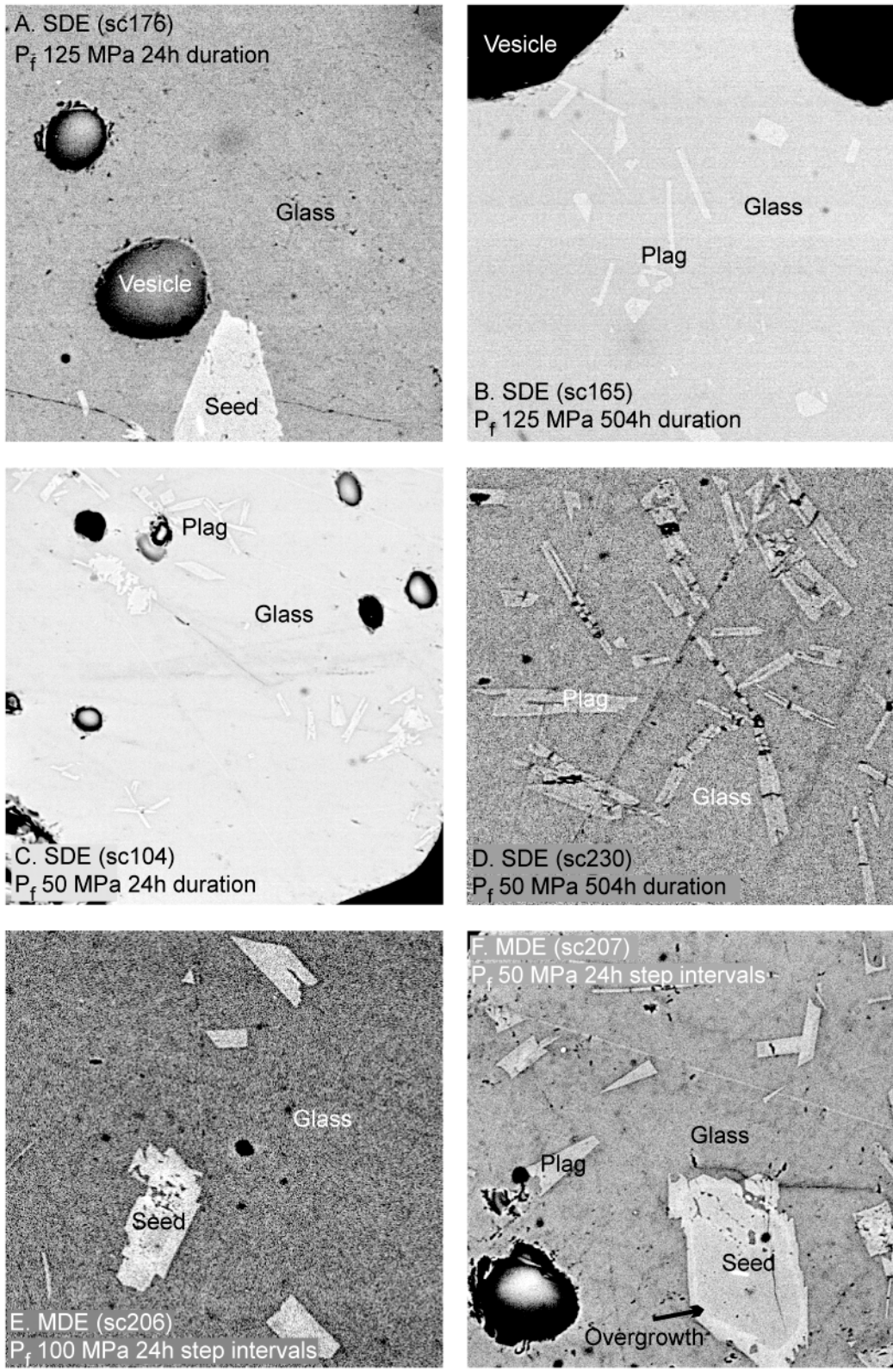

FIGURE 5. Back-scattered electron images of SDE experiments using haplogranite composition. P_f, final pressure, and duration of experiment as labeled. Characteristic morphologies and seed crystals are indicated. All fields of view = 200 μm.

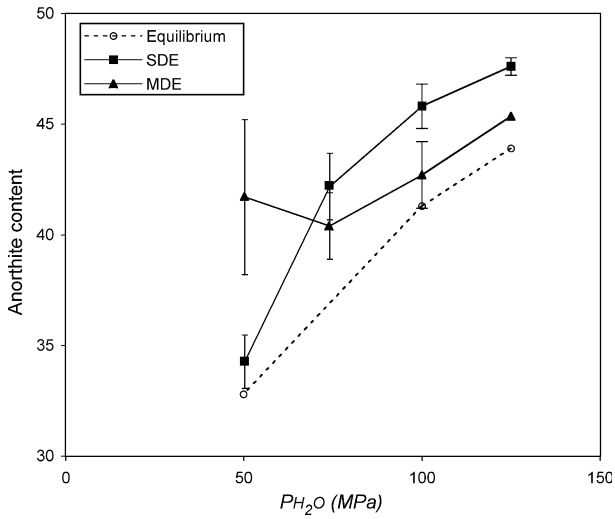

FIGURE 6. Comparison of plagioclase anorthite contents from equilibrium and decompression experiments run at 875 °C. Plagioclase compositions from the longest experiments were used (±1σ of mean anorthite content shown).

mences after at least 8 hours, and at high undercoolings, crystallization starts after at least 4 hours. For the MDE, the fraction of plagioclase crystallized increases with time and ΔT in most cases. The highest proportion of plagioclase is found in the experiment with the longest duration and highest total undercooling. The MDE crystallize considerably less plagioclase than the SDE for the same ΔT_{total} (Fig. 8). Comparison of the plagioclase fraction from the decompression and equilibrium experiments suggests that the decompression experiments consistently crystallize less plagioclase (Fig. 9).

Crystal number density. The crystal number density is observed to increase with ΔT for SDE experiments with durations of 8 hours or longer (Fig. 10). For the SDE, there is a modest increase in the number of sites with time, and for the MDE, there is some correlation between crystal density and experimental duration. The SDE consistently nucleate more plagioclase sites than the MDE at the same P_f. It was observed, on a qualitative basis, that there was considerable heterogeneity in the distribution of crystal sites; some images contained numerous crystals, whereas others were devoid of crystals, with this variability being reflected in the high calculated standard deviations (Table 4). There was no correlation between images that included seed crystals and images that contained decompression-induced crystallization. There is evidence to suggest that some nucleation was heterogeneous, utilizing seed crystals and also vesicles, but no evidence for crystallization nucleated at the container wall.

Nucleation lag. By using compositional and textural data, minimum nucleation lags can be estimated for each undercooling. The low proportion of plagioclase, both in terms of area fraction and nucleation density within the 1 and 4 hour experiments, suggests that nucleation only commenced after 4 hours. Therefore, for all undercoolings (ΔT = 35–167 °C), the nucleation lag is considered to be at least 4 hours.

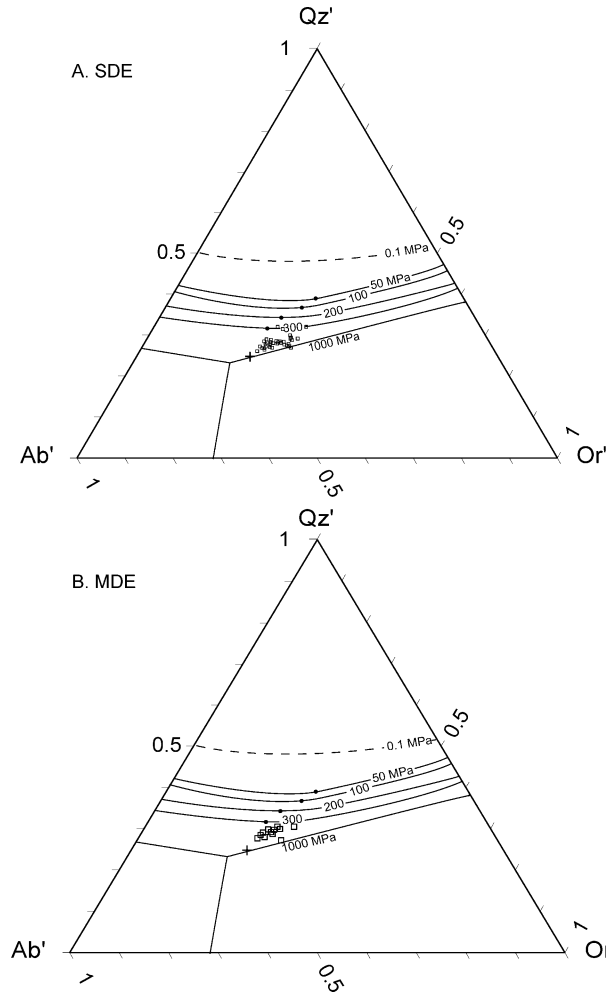

FIGURE 7. Decompression experiment glass compositions projected into albite-quartz-orthoclase ternary. (**A**) single-decompression experiments (**B**) multi-decompression experiments. Cross-starting composition; open squares = quartz-absent experiments.

Nucleation rate. Nucleation rate was calculated using a nucleation delay of 4 hours. For both SDE and MDE, the nucleation rate increases with ΔT (Fig. 11), and the maximum nucleation rate was not identified over the range of experimental conditions. For the SDE, nucleation predominantly took place within 8 hours, with essentially insignificant nucleation after this time. The MDE experiments have lower nucleation rates than SDE, and the nucleation rate is highest in the experiments with a short duration or low P_f.

Growth rate. For both types of experiment, the maximum crystal length increases with time and ΔT (Fig. 12). For the SDE, the increase in crystal length for a given ΔT is greatest in the 16 hours following the nucleation lag. For the MDE, the crystal length increases with experimental duration and ΔT.

Maximum growth rate varies as a function of ΔT (Fig. 13). For the SDE, the calculated growth rate is incremental, whereas for the MDE, it is time-averaged. The growth rate for the SDE increases with undercooling, reaching a maximum at $\Delta T \sim 100$ °C, and then decreasing at higher ΔT. The crystallization be-

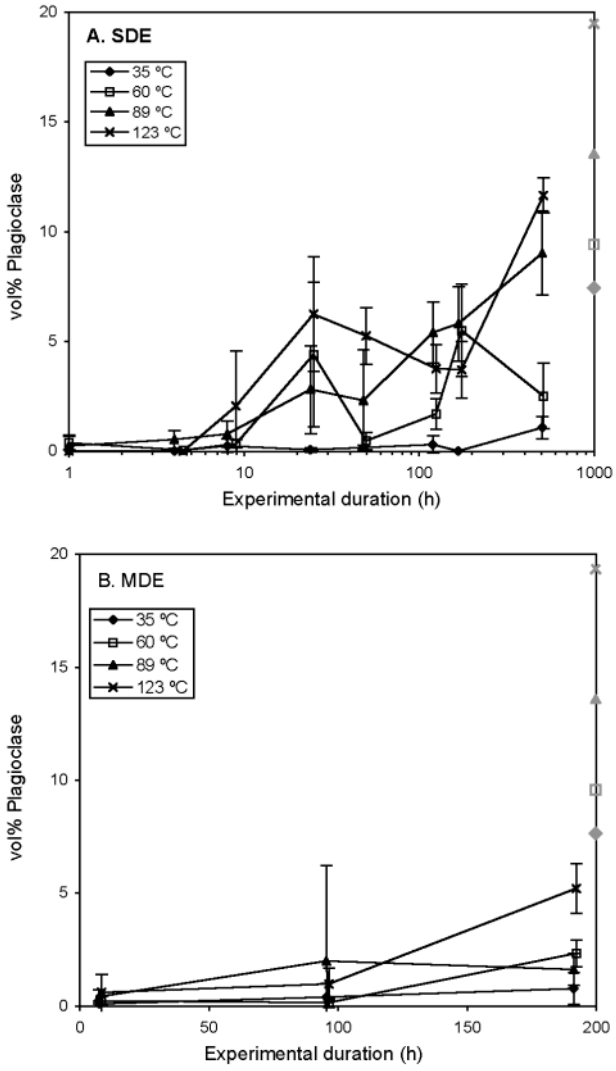

FIGURE 8. Graph of plagioclase fraction as a function of time for given ΔT. On the right-hand axis, the equilibrium plagioclase fraction for the given P_f is shown, and $\pm 1\sigma$ of mean plagioclase fraction is shown with slight offset for clarity.

havior of the system is characterized by a 4 hour lag, followed by rapid growth for 4 hours, and then little further growth. For the MDE, there is also a peak in growth rate at $\Delta T \sim 100$ °C, and the highest growth rates have been calculated for the short-duration experiments.

The SDE growth and nucleation rates can be considered in terms of the effective undercooling, which is an estimate of the likely undercooling still imposed after some crystallization has taken place. The effective undercooling is calculated from the bulk crystallinity of a given experiment, which in turn is determined by mass-balance calculations based on the melt composition. Using this procedure, the position of the plagioclase liquidus after this crystallization can be approximated. Therefore, the effective undercooling represents the difference between the shifted plagioclase liquidus following crystallization and the conditions of the experiment. The effective undercooling should trend toward zero as equilibrium is reached. As effective ΔT decreases, both nucleation and growth rates decrease as the system tends toward equilibrium (Fig. 14); however, neither reaches zero undercooling over the duration of experiments considered.

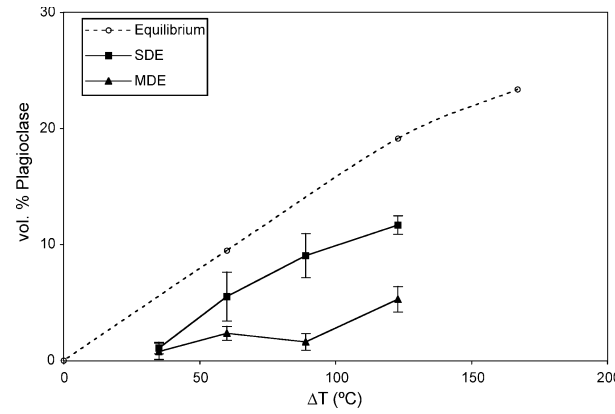

FIGURE 9. Comparison of plagioclase fraction for equilibrium and decompression experiments as a function of ΔT. For the decompression experiments, the plagioclase fraction for the longest duration experiment was used ($\pm 1\sigma$ of mean plagioclase fraction shown).

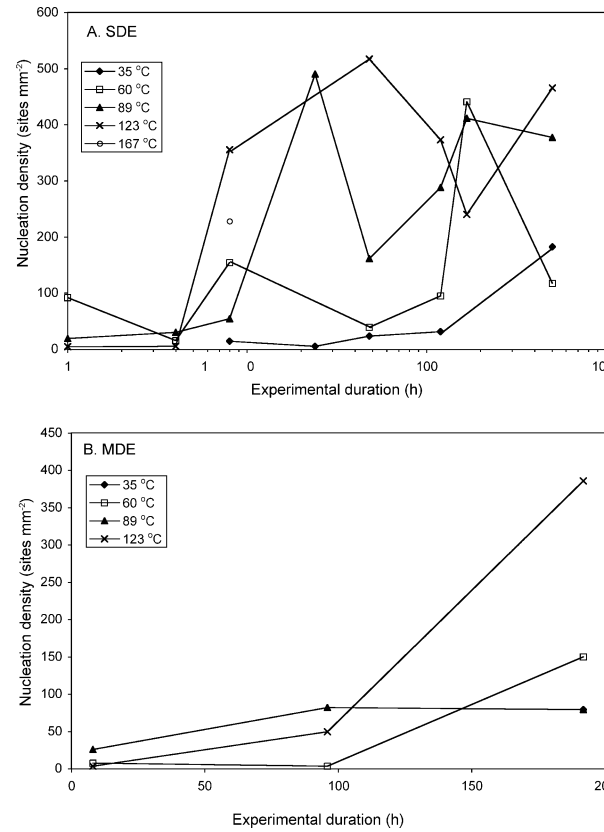

FIGURE 10. Graphs of the relationship between nucleation density and experimental duration as a function of ΔT (°C).

Maximum overgrowth thickness. For both types of ex-

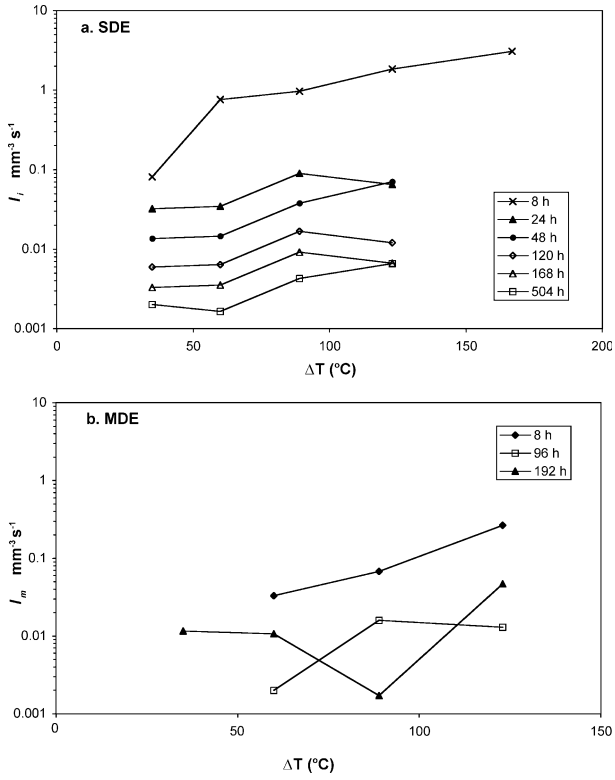

FIGURE 11. Graphs of nucleation rate (I) as a function of undercooling (ΔT) with experimental duration (in hours).

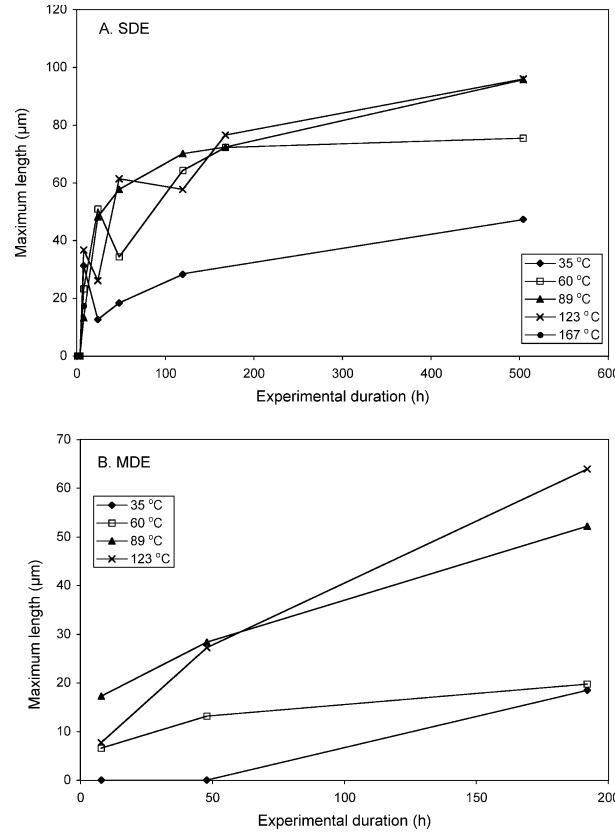

FIGURE 12. Graph of maximum crystal length with experimental duration as a function of ΔT. The length represents the average of the 10 longest crystals formed during decompression.

periment, the maximum observed rim thickness increases with time and ΔT (Fig. 15). In some cases, the 5 images selected did not contain any seed crystals; therefore, overgrowth rims could not be measured. The overgrowth rims are considerably thinner than the maximum observed crystal lengths, implying that growth rates must have been slower on the overgrowths. The new crystals are likely to represent growth along the fastest-growing crystal axis, whereas the overgrowth rims represent growth over different crystallographic axes.

Repeat experiments. Comparison of repeat experiments shows that there is good agreement in terms of amount of plagioclase crystallized, its anorthite content, and maximum estimated growth rates (Table 4). There is less agreement in terms of nucleation density or maximum crystal length; however, both of these are highly variable measures sensitive to slight variations in P-T conditions. Overall the repeat experiments suggest reasonable reproducibility of both single-step and multi-step experiments.

DISCUSSION OF DECOMPRESSION EXPERIMENTS

The decompression experiments have shown the effect of depressurization on a haplogranite melt. As P_f decreases, and therefore ΔT increases, there is nucleation and growth of new crystal sites. The rate of crystallization was found to depend on the magnitude of ΔT. Crystal fraction, nucleation rate, and growth rate all increase with ΔT, although at high ΔT, the growth rate peaks and then begins to decrease.

Comparison of the SDE and MDE shows that the amount of undercooling experienced at a given stage will control the crystallization kinetics, rather than the total ΔT experienced. For example, the SDE consistently crystallized more plagioclase than the MDE for the same ΔT_{total} and the same experimental duration (Fig. 8). The SDE also produce higher nucleation densities and faster maximum growth rates.

Using equilibrium glass and plagioclase composition data, a binary loop of the simple An-Ab system can be approximated (Fig. 16a). Comparison of the equilibrium and decompression experiments (Fig. 16b) shows that, for both SDE and MDE, equilibrium was not approached. It is likely that part of the offset relative to the equilibrium experiments is due to resorption of the seed crystals. Experimental studies on resorption rates of feldspar (Wark and Stimac 1992) indicate that 40 μm thick dissolution zones can form within 4 hours. Therefore it is possible that resorption of the seed crystals occurs during the 4–8 hour nucleation lag, changing the melt composition. This phenomenon explains the low K_2O contents observed in some of the experimental glass compositions.

The haplogranite system has relatively sluggish crystallization kinetics, with a nucleation lag of at least 4 hours, regardless of the degree of undercooling. Once nucleation commences, the majority of growth occurs over the following 20 hours and, thereafter, crystal growth rates decrease. Over the range of experimental durations considered (1–504 h),

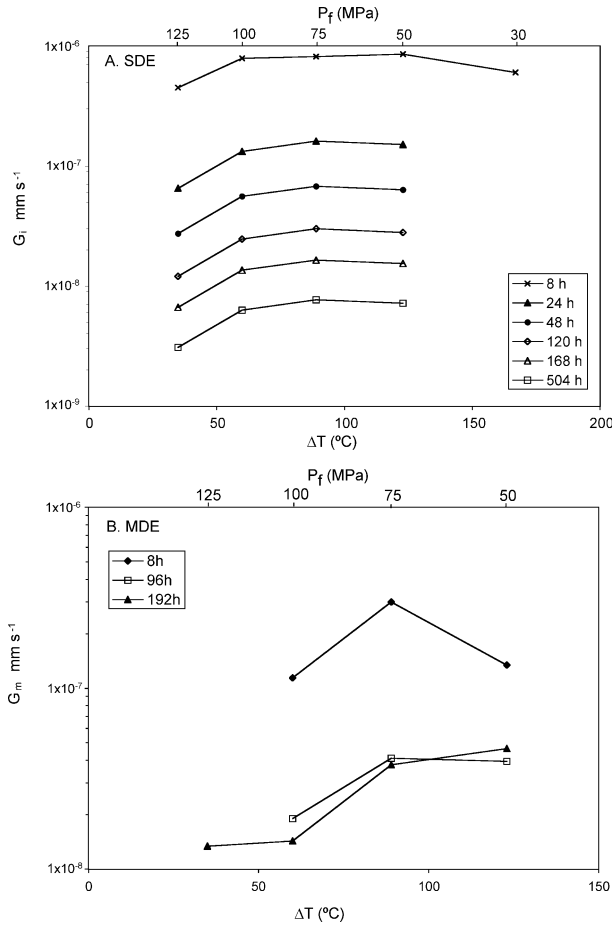

FIGURE 13. Graph of maximum growth rate as a function of undercooling for varying experimental durations using the haplogranite composition. Growth rate calculated using the average of the half-length of the 10 longest new growth crystals in an experiment and is calculated incrementally for SDE and is a time average for the MDE.

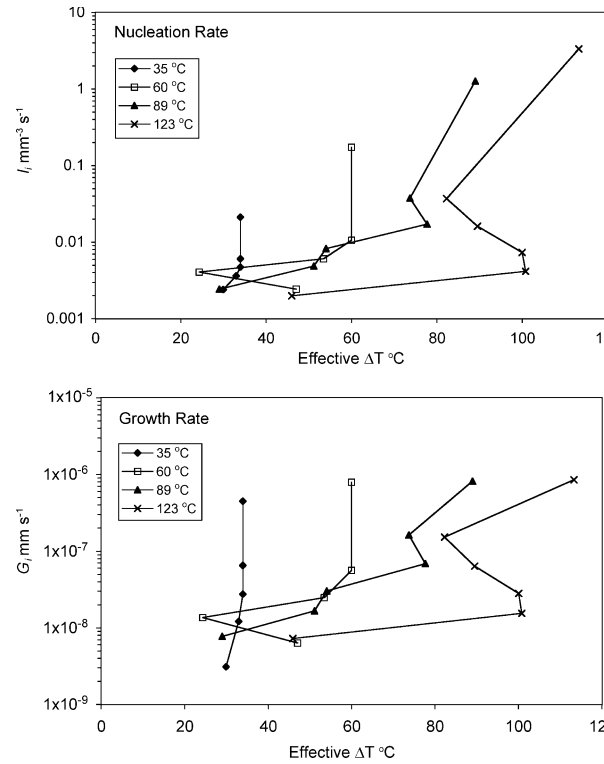

FIGURE 14. Growth rates and nucleation rates for SDE as a function of effective ΔT.

equilibrium was not approached. This is shown by the absence of phases, lower crystal fractions, and also by calculations of evolving ΔT (Fig. 14), which suggest that the effective ΔT never reaches zero.

Another consideration when interpreting the crystallization kinetics is the water content and its effect on melt viscosity. For the decompression experiments, as pressure decreases, the amount of water that can be dissolved in the melt will decrease. This decrease has a strong influence on the melt viscosity, which in turn will control rates of diffusion of components and crystallization kinetics (Kirkpatrick 1981). The variation in melt viscosity with pressure can be calculated using Shaw (1974) with melt compositions and estimated water contents (Table 6). The melt composition is estimated using the starting haplogranite composition, which is recalculated allowing for the estimated water content at the pressure of interest. There is a marked increase in viscosity as pressure and water content decrease. The increasing viscosity should result in sluggish crystallization kinetics; however, this will be balanced by increasing ΔT driving crystallization.

COMPARISON WITH OTHER STUDIES

Swanson (1977) used a similar haplogranite composition (Table 1) to determine nucleation densities and rates of crystal growth as a function of cooling. Capsules of starting material and H_2O were annealed at 1000 °C for at least 96 hours before being cooled to the temperature of interest over several minutes and then left for 1–6 days. The experiments contained 3.5 wt% H_2O, and therefore were not water-saturated at the run pressure of 800 MPa. Due to a lack of crystallization in some of the experiments of Swanson, the nucleation rate could not be calculated. Both studies suggest similar maximum values of nucleation density and growth rate (Fig. 17); however, the peak is found at a lower undercooling for the results of this study.

There are differences in the ways that the nucleation density and growth rates were estimated in the two studies. Swanson took the experimental products and examined them with an optical microscope, permitting 3-D analysis. Estimates of the experimental charge volume were used to determine the nucleation density, whereas this study used back-scattered electron images. Swanson did not allow for a nucleation lag and, hence, his growth rate estimates are likely to be minimum values. However as the full crystal length could be measured in every case, crystal sizes were probably larger relative to the sizes measured in this study. Nevertheless, these differences in methodology are unlikely to fully explain the variation in results.

Davis et al. (1997) discussed the influence of water content

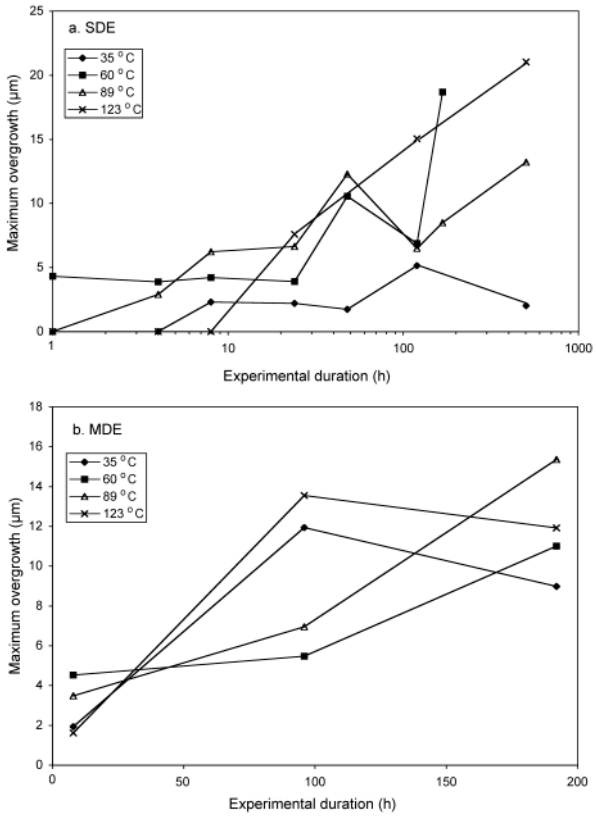

FIGURE 15. Graph of maximum overgrowth rim width against experimental duration as a function of undercooling. Rims measured on overgrowths of seed crystals.

TABLE 6. Calculation of melt viscosity for haplogranite at varying final pressure and ΔT using Shaw (1974)

P_f	Haplogranite	125	100	75	50	Swanson
ΔT	composition	35	69	89	123	composition
SiO_2	72.93	69.13	69.57	69.94	70.67	71.39
Al_2O_3	15.88	15.06	15.15	15.23	15.39	14.54
CaO	1.70	1.61	1.62	1.63	1.65	1.45
Na_2O	3.80	3.60	3.62	3.64	3.68	3.62
K_2O	5.69	5.40	5.43	5.46	5.52	5.50
H_2O	0.00	5.21	4.60	4.10	3.10	3.50
ln η (poise)	22.39	11.81	12.65	13.39	15.05	14.43

Notes: The water content the average of all water contents for the given P_f as determined by the by-difference method (Devine et al. 1995). P_f of 30 MPa is not calculated as there is insufficient data to estimate the water content. The melt viscosity of the Swanson composition is also calculated.

on nucleation kinetics, finding that increased water content aids nucleation of crystals. The decompression experiments of this study were water-saturated whereas the Swanson experiments were undersaturated. By adding water, crystallization can be initiated at much lower degrees of undercooling, which can explain the high nucleation densities and growth rates estimated in this work. As discussed, the water content will strongly affect diffusion processes, making it far easier to transport the components needed to form crystals at high water contents.

This view is supported by the comparison with the other experimental compositions used by Swanson in his 1977 study.

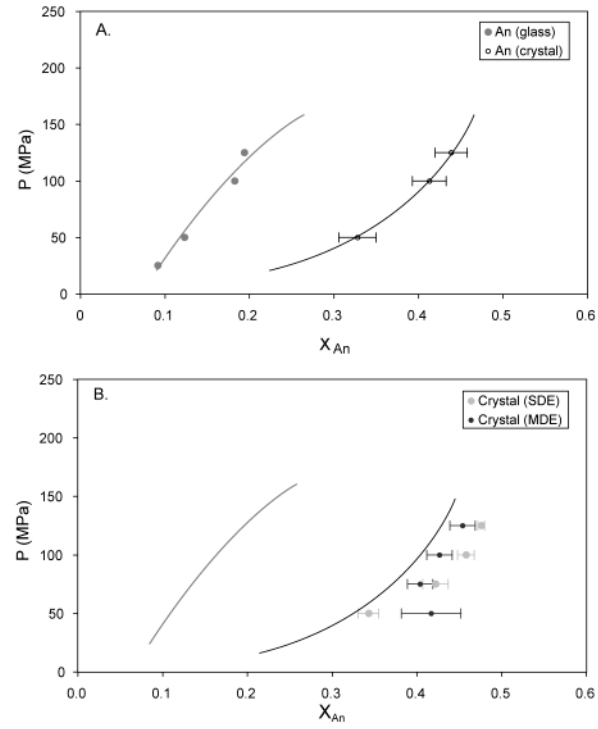

FIGURE 16. (**a**) Experimental isothermal phase diagram, using equilibrium glass compositions and equilibrium plagioclase anorthite content as a function of pressure. All experiments were run at 875 °C. (**b**) SDE and MDE plagioclase compositions plotted in comparison to equilibrium loop.

Two sets of experiments were run using a granodiorite composition and varying water contents (6.5 and 12 wt% H_2O). Results suggest that adding water results in faster nucleation and growth rates at lower degrees of undercooling. The situation is further complicated, as some of the experiments carried out in this study were decompressed to less than 75 MPa and therefore contain less water than the experiments of Swanson. Hence, the estimated melt viscosity is higher for the haplogranite than the Swanson experiments (Table 6), which should result in slower crystallization kinetics, although this is not observed.

Couch et al. (2003b) studied the crystallization kinetics of decompression-induced crystallization for the andesite of the Soufrière Hills Volcano, Montserrat. Experiments were performed with an analogue representative groundmass composition (71 wt% SiO_2). The experimental and analytical procedure was identical to the haplogranite study. Comparison with the Montserrat study suggests that the haplogranite has sluggish crystallization kinetics (Fig. 18), as there is a greater nucleation lag, and lower nucleation and growth rates for the haplogranite system. The melt viscosity of the Montserrat groundmass melt was estimated using the method of Shaw (1974), and was found to vary from ln η 8.8–13.71 poise over a similar experimental range to the haplogranite. Clearly, the melt viscosity of the haplogranite is always greater at similar experimental conditions, resulting in slower diffusion rates and, therefore, more sluggish crystallization kinetics.

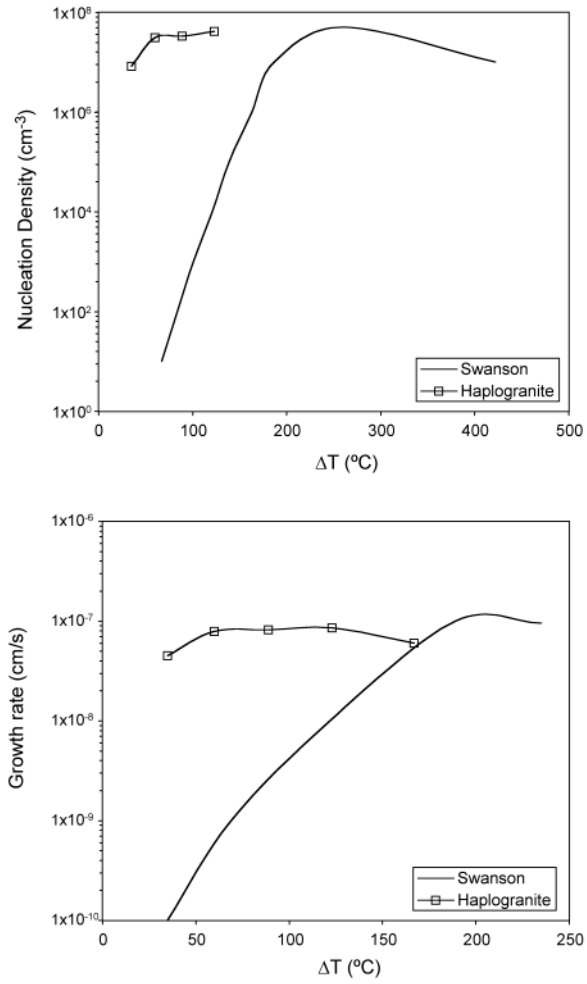

FIGURE 17. Comparison of maximum nucleation density and growth rate estimated in this study (labeled as haplogranite) with data from experiments of Swanson (1977) using a similar composition.

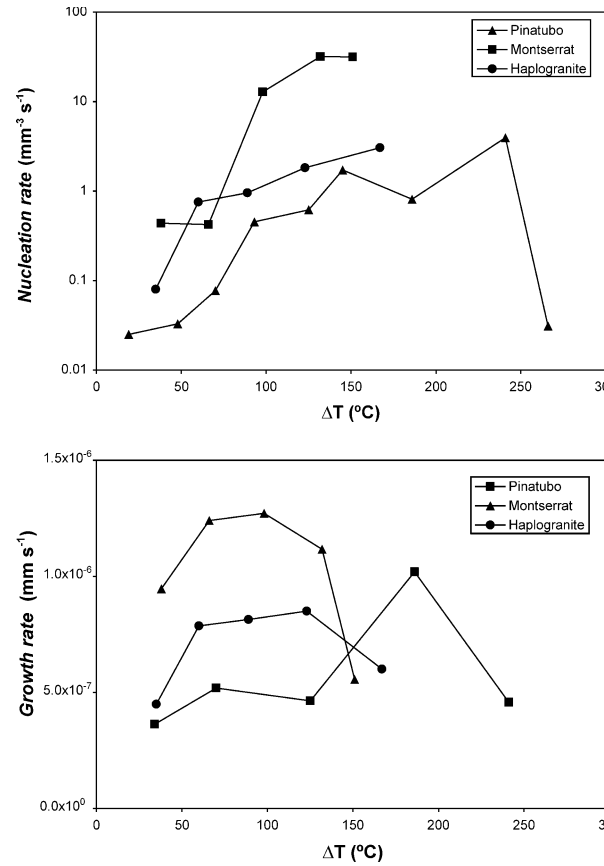

FIGURE 18. Comparison of maximum nucleation and growth rates for several experimental studies. Data for Pinatubo (78 wt% SiO_2) from Hammer and Rutherford (2002) and Montserrat (71 wt% SiO_2) from Couch et al. (2003b).

Hammer and Rutherford (2002) performed decompression experiments on Pinatubo dacite to study feldspar crystallization kinetics. The starting material was crushed pumice, containing phenocrysts and glass with 78 wt% SiO_2 (anhydrous). Experiments were annealed at high pressure and then decompressed either in single- or multi- decompression steps. Comparison with these results (Fig. 18), suggests that the Pinatubo system requires higher values of ΔT to produce similar nucleation and growth rates. However, at high ΔT, the rates of nucleation and growth exceed those of the haplogranite. It should be noted that Hammer and Rutherford did not allow for a nucleation lag period and, therefore, the data are likely to underestimate the rates of nucleation and growth. The higher SiO_2 content of the Pinatubo dacite results in generally higher melt viscosities [ln η ~10.4–17.7 poise, using the method of Shaw (1974) with compositional data from Hammer and Rutherford (2002)] than the haplogranite, which may explain the high ΔT required for crystallization of the dacite.

It seems that the presence of minor components such as Mg and Fe may have a role in influencing crystallization kinetics. Peak rates of nucleation and growth are higher in the experimental studies that contained these minor components (Montserrat and Pinatubo) regardless of SiO_2 content, than in the Fe- and Mg-free haplogranite. A minor factor to consider is that the Pinatubo dacite experiments used a natural starting material, whereas the haplogranite and Montserrat andesite studies both used analogue compositions. It is not altogether clear how these impurities influence the crystallization kinetics, although there may be differences in melt heterogeneities that could affect rates of nucleation and growth (Naney and Swanson 1980).

From comparison with several experimental studies, it is clear that several factors influence crystallization kinetics. Increasing SiO_2 results in sluggish kinetics, as shown by the higher ΔT required to reach peak crystallization rates (Fig. 18). There is evidence from comparison with the haplogranite and the experiments of Swanson that higher water content aids crystallization by lowering the melt viscosity. These compositional controls are counterbalanced by the increasing disequilibrium experienced as ΔT increases. Hence, the haplogranite system, with moderate SiO_2 and H_2O content relative to other studies

considered, is slow to crystallize at low ΔT, as the melt viscosity is relatively high. As ΔT increases and water content decreases, melt viscosity will increase further; however, the extent of disequilibrium is sufficient to overcome the sluggishness, resulting in crystallization.

ACKNOWLEDGMENTS

The author acknowledges a NERC studentship. Useful discussions with Steve Sparks are gratefully acknowledged. Careful reviews by Kathy Cashman and Don Baker helped to clarify the work considerably.

REFERENCES CITED

Bachmann, O., Dungan, M.A., and Lipman, P.W. (2002) The Fish Canyon magma body, San Juan volcanic filed, Colorado: rejuvenation and eruption of an upper crustal batholithic magma chamber. Journal of Petrology, 43, 1469–1503.

Blundy, J. and Cashman, K.V. (2001) Magma ascent and crystallization at Mount St Helens, 1980-1986. Contributions to Mineralogy and Petrology, 140, 631–650.

Carroll, M.R. and Blank, J.G. (1997) The solubility of H_2O in phonolitic melts. American Mineralogist, 82, 549–556.

Cashman, K.V. and Blundy, J. (2000) Degassing and crystallization of ascending andesite and dacite. Philosophical Transactions of the Royal Society of London A, 358, 1487–1513.

Cheng, H.C. and Lemlich, R. (1983) Errors in the measurement of bubble size distribution in foam. Industrial Engineering Chemical Fundamentals, 22, 105–109.

Couch, S., Harford, C.L., Sparks, R.S.J., and Carroll, M.R. (2003a) Experimental constraints on andesite petrogenesis at the Soufrière Hills Volcano, Montserrat. Journal of Petrology, 44, 1455–1475.

Couch, S., Sparks, R.S.J., and Carroll, M.R. (2003b) The kinetics of degassing-induced crystallization at Soufrière Hills Volcano, Montserrat. Journal of Petrology, 44, 1477–1502.

Davis, M.J., Ihinger, P.D., and Lasaga, A.C. (1997) Influence of water on nucleation kinetics in silicate melt. Journal of Non-Crystalline Solids, 219, 62–69.

Delaney, J.R. and Karsten, J.L. (1981) Ion microprobe studies of water in silicate melts: concentration-dependent water diffusion in obsidian. Earth and Planetary Science Letters, 52, 191–202.

Devine, J.D., Gardner, J.E., Brack, H.P., Layne, G.D., and Rutherford, M.J. (1995) Comparison of microanalytical methods for estimation H_2O contents of silicic volcanic glasses. American Mineralogist, 80, 319–328.

Eichelberger, J.C., Carrigan, C.R., Westrich, H.R., and Price, R.H. (1986) Non-explosive silicic volcanism. Nature, 323, 598–602.

Fenn, P.M. (1977) The nucleation and growth of alkali feldspars from hydrous melts. Canadian Mineralogist, 15, 135–161.

Gardner, J.E., Hilton, M., and Carroll, M.R. (2000) Bubble growth in highly viscous melts during continuous decompression from high pressure. Geochimica et Cosmochimica Acta, 64, 1473–1483.

Geschwind, C.H. and Rutherford, M.J. (1995) Crystallisation of microlites during magma ascent: the fluid mechanics of 1980-1986 at Mount St Helens. Bulletin of Volcanology, 57, 356–370.

Hammer, J.E. and Rutherford, M.J. (2002) An experimental study of the kinetics of decompression-induced crystallization in silicic melt. Journal of Geophysical Research, 107, 148–227.

Hammer, J.E., Cashman, K.V., Hoblitt, R.P., and Newman, S. (1999) Degassing and microlite crystallization during pre-climatic events of the 1991 eruption of Mt. Pinatubo, Philippines. Bulletin of Volcanology, 60, 355–380.

Kellerhals, R., Shaw, J., and Arora, V.K. (1975) On grain size from thin sections. Journal of Geology, 83, 79–96.

Kirkpatrick, R.J. (1981) Kinetics of crystallisation in igneous rocks. In A.C. Lasaga and R.J. Kirkpatrick, Eds., Kinetics of Geochemical Processes, 8, 321–397. Reviews in Mineralogy, Mineralogical Society of America, Washington, D.C.

Lejeune, A.-M. and Richet, P. (1995) Rheology of crystal-bearing silicate melts: an experimental study at high viscosities. Journal of Geophysical Research, 100, 4215–4229.

Mastin, L.G. and Ghiorso, M.S. (2001) Adiabatic temperature changes of magma-gas mixtures during ascent and eruption. Contributions to Mineralogy and Petrology, 141, 307–321.

Melnik, O. and Sparks, R.S.J. (1999) Nonlinear dynamics of lava dome extrusion. Nature, 402, 37–41.

Naney, M.T. and Swanson, S.E. (1980) The effect of Fe and Mg on crystal growth in synthetic granitic and granodioritic liquids. American Mineralogist, 65, 639–653.

Navon, O. and Lyakhovsky, V. (1998) Vesiculation processes in silicic magmas. In J.S. Gilbert and R.S.J. Sparks, Eds., The physics of explosive volcanic eruptions. London, Geological Society. 145, 27–50.

Nockholds, S.R. (1954) Average chemical composition of some igneous rocks. Geological Society of America Bulletin, 65, 1007–1032.

Rutherford, M.J., Sigurdsson, H., Carey, S., and Davis, A. (1985) The May 18, 1980, eruption of Mount St Helens 1. Melt composition and experimental phase equilibria. Journal of Geophysical Research, 90, 2929–2947.

Rutherford, M.J., Devine, J.D., and Barclay, J. (1998) Changing conditions and ascent rates during the Soufrière Hills eruption on Montserrat. GSA Today, 8, 1–7.

Sahagian, D. and Proussevitch, A. (1996) Thermal effects of magma degassing. Journal of Volcanology and Geothermal Research, 74, 19–38.

Shaw, H.R. (1974) Diffusion of H2O in granitic liquids: Part 1. Experimental data. In A.W. Hofmann, Ed., Geochemical transport and kinetics, 68, 6337–6343. Carnegie Institute, Washington, D.C.

Silver, L.A., Ihinger, P.D., and Stolper, E. (1990) The influence of bulk composition on the speciation of water in silicate glasses. Contributions to Mineralogy and Petrology, 104, 142–162.

Sparks, R.S.J., Murphy, M.D., Lejeune, A.-M., Watts, R., Barclay, J., and Young, S.R. (2000) Control on the emplacement of the andesite lava dome of the Soufrière Hills volcano by degassing-induced crystallisation. Terra Nova, 12, 14–20.

Swanson, S.E. (1977) Relation of nucleation and crystal-growth rate to the development of granitic textures. American Mineralogist, 62, 966–978.

Taylor, J.R., Wall, V.J., and Pownceby, M.I. (1992) The calibration and application of accurate redox sensors. American Mineralogist, 77, 284–295.

Tuttle, O.F. and Bowen, N.L. (1958) Origin of granite in the light of experimental studies. 153 p, Geology Society of America, Boulder, Colorado.

Voight, B., Sparks, R.S.J., Miller, A.D., Stewart, R.C., Hoblitt, R.P., Clarke, A.B., Ewert, J.W., Aspinall, W.P., Baptie, B., Calder, E.S., Cole, P., Druitt, T.H., Harford, C., Herd, R.A., Jackson, P., Lejeune, A.-M., Lockhart, A.B., Loughlin, S., Luckett, R., Lynch, L., Norton, G.E., Robertson, R.E., Watson, I.M., Watts, R., and Young, S.R. (1999) Magma flow instability and cyclic activity at Soufrière Hills Volcano, Montserrat, British West Indies. Science, 283, 1138–1142.

Wark, D.A. and Stimac, J.A. (1992) Origin of mantled (rapakivi) feldspars—experimental-evidence of a dissolution-controlled and diffusion-controlled mechanism. Contributions to Mineralogy and Petrology, 111, 345–361.

Weibel, E.R. (1980) Stereological Methods, volume 2. Theoretical foundations, Academic Press.

Whitney, J.A. (1975) The effects of pressure, temperature and X_{H2O} on phase assemblage in four synthetic rock compositions. Journal of Geology, 83, 1–31.

Wright, T.L. and Doherty, P.C. (1970) A linear programming and least squares computer method for solving petrologic problems. Geological Society of America Bulletin, 81, 1995–2008.

Wylie, J.J., Voight, B., and Whitehead, J.A. (1999) Instability of magma flow from volatile-dependent viscosity. Science, 285, 1883–1885.

Zhang, Y.X. (1999) Exsolution enthalpy of water from silicate liquids. Journal Of Volcanology and Geothermal Research, 88, 201–207.

MANUSCRIPT RECEIVED SEPTEMBER 2, 2002
MANUSCRIPT ACCEPTED APRIL 1, 2003
MANUSCRIPT HANDLED BY JOHN AYERS